Plasma Physics and
Controlled Fusion

PAPER • **OPEN ACCESS**

First field test of a novel optical gas analyser in the exhaust of Wendelstein 7-X

To cite this article: G Schlisio *et al* 2026 *Plasma Phys. Control. Fusion* **68** 035029

Plasma Physics and Controlled Fusion

OPEN ACCESS

RECEIVED
30 September 2025

REVISED
20 February 2026

ACCEPTED FOR PUBLICATION
16 March 2026

PUBLISHED
26 March 2026

PAPER

First field test of a novel optical gas analyser in the exhaust of Wendelstein 7-X

G Schlisio[1,*], J Brindley[2], M Law[2], C C Klepper[3], E Delabie[3], T Bräuer[1], P Zs Pölöskei[1], Y M Boumendjel[1], F B T Siddiki[4,1], M Krychowiak[1] and the W7-X team[5]

[1] Max-Planck-Institut für Plasmaphysik, Wendelsteinstraße 1, 17491 Greifswald, Germany
[2] Gencoa Ltd, 4 De Havilland Drive, Estuary Commerce Park, Liverpool L24 8RN, United Kingdom
[3] Oak Ridge National Laboratory, Oak Ridge, TN 37831, United States of America
[4] UW Madison, 1500 Engineering Drive, Madison, WI 53706, United States of America
[5] See Grulke *et al* 2024 (https://doi.org/10.1088/1741-4326/ad2f4d) for the W7-X team.
[*] Author to whom any correspondence should be addressed.

E-mail: georg.schlisio@ipp.mpg.de

Keywords: magnetic confinement fusion, vacuum, spectroscopy

Abstract

A novel optical gas analyser, designed for isotope-resolved exhaust composition measurement, was field-tested at Wendelstein 7-X (W7-X) to validate its laboratory-proven concept under operational fusion experiment conditions. The system, Optix, comprises a cold cathode remote plasma generator and a high-resolution Fabry–Perot spectrometer and was deployed in the exhaust line of W7-X during the OP2.3 campaign. The injection of ^{3}He and ^{4}He for minority ion-cyclotron heating provided a test case for helium isotope discrimination. Despite limitations due to background gas and low partial pressures of the target species, isotope-resolved spectral signatures were successfully observed, demonstrating the fundamental viability of the Optix approach. Additionally, the spectrometer was evaluated for plasma emission measurements from both core and edge sightlines. While helium line emission was detectable, interpretation was hindered by complex background signals, highlighting the benefits of controlled remote plasma generators for spectroscopy. This first deployment provides critical insight into pressure requirements, spectral resolution, and operational constraints, informing future applications of optical exhaust diagnostics in fusion devices.

1. Introduction

Exhaust composition measurement in magnetic confinement fusion experiments, and especially future reactors, is an essential task for inventory accounting. Mass spectrometry methods rely on free-streaming charged particles in sensitive electrode array, and are susceptible to residual magnetic field interference. Optical gas analysers (OGAs) follow a different approach, by spectroscopically observing a private low-temperature plasma generated locally from the exhaust gas. For this purpose, a low-temperature plasma is usually generated in a cold cathode discharge.

The OGA presented in this work was originally developed for commercial vacuum process control by Gencoa Ltd. [1, 2], and has been equipped with a custom high-resolution spectrometer for isotope measurement relevant for fusion experiments. The system will be referred to as Optix throughout this document, to distinguish it from the classical OGA (cOGA) - a combination of an Alcatel CF2 Penning source with a filterscope observation system widely used in fusion experiments [3–6]. An existing cOGA was not operable during the presented work.

Wendelstein 7-X (W7-X) [7] is the largest stellarator experiment in operation, and has conducted its operational phase 2.3 (OP2.3) in 2025. A wide variety of topics was investigated during OP2.3, resulting in 2746 plasma programs with a total duration of 678 min and a maximum energy turnover of 1.8 GJ. An overview of the obtained plasma parameters is given in [8]. As W7-X is currently not operating in

deuterium nor tritium, the planned injection of ^{3}He for ion-cyclotron minority heating [9, 10] was used as a test-case for isotope resolution in the W7-X OP2.3. The potential for isotopically resolving helium with an OGA technique was very recently demonstrated [11].

The goal of the reported investigation was to test the Optix in a fusion experiment under field conditions, which differ from laboratory conditions in many ways.

The experimental setup is described in section 2, section 3 discusses the challenges and solutions with the sampled gas pressure. The helium isotope measurement is shown in section 4, and section 5 explores the further application of the involved spectrometer for plasma spectroscopy.

2. Setup

The basic principle of the optical gas detection method is that gas molecules enter the plasma generator and are excited by free electrons or other energetic gas species. This results in light emission at wavelengths attributable to the gas molecules, with the light intensity proportional to the gas concentration. Thus, a light emission spectrum corresponding to detected gas species is formed, in contrast to the mass spectrum as generated by a mass spectrometer.

The Optix consists of a remote plasma generator and an observing spectrometer. The remote plasma generator consists of a inverted magnetron gauge operated constant-current mode with a standard current of 200 μA, which is observed via an optical fibre with a 600 μm core and an $NA = 0.5$.

The spectrometer—a custom Fabry–Perot spectrometer (FPS) by LightMachinery—was set up for the ^{4}He I line at 667.8151 nm with an approximate spectral range of about 110 pm, an optical resolution of about 11 pm and a digitalization resolution of 0.9 pm. The basic principle of a FPS is the self-interference of the analysed light in a parallel glass plate (etalon) with a high-precision thickness. Multiple internal reflections at the partially reflective surfaces lead to wavelength-selective transmission according to the resonance condition set by the plate thickness and refractive index. The spectrum is obtained from the angularly resolved transmission pattern, since each wavelength is transmitted at a specific incidence angle. An in-depth discussion of the principle and its applications is given in [12].

Both the spectrometer camera and the remote plasma generator were controlled with a standard PC, which was integrated into the control system of W7-X to automatically detect running experiment programs and upload both raw and processed data to the data archive [13].

The Optix was hosted on the diagnostic residual gas analyser (DRGA) [14, 15], where a dedicated OGA vacuum chamber (Optix Pos.1) is located at an interstage port of the turbo-molecular pump (TMP). At the OGA chamber the cOGA was operated previously, but with very low light attributed to pressures below $1{\cdot}10^{-4}$ mbar. A secondary vacuum line from the OGA chamber to the backing line was installed to benefit from higher pressures in the exhaust stream of the TMP. The vacuum connections of the OGA chamber to the exhaust gas stream are each equipped with a valve and only one is opened at a time. To further increase the pressure in the OGA chamber, a throttle valve was introduced between the OGA chamber and the roughing pump. In a second step, the Optix was moved away from the OGA chamber and mounted directly on the main roughing line of the W7-X pumping system where a higher gas throughput was observed (Optix Pos.2). Further discussion on the rationale and results of this move are given in section 3. A detailed schematic drawing of the setup including all relevant valves, identifiers, and both Optix mounting positions is shown in figure 1.

Due to the thermal expansion of the etalon inside the FPS, the wavelength calibration of the setup was sensitive to temperature changes of the spectrometer. This requires a temperature-dependent wavelength correction of the obtained spectra by matching identified peaks with expected signals at a known wavelength. This approach yielded a correction of typically less than 10 pm. In the following, all spectra are shown temperature-corrected unless otherwise noted. Temperature-controlling the etalon presents a viable solution for future spectrometers, which will remove the necessity of temperature-correcting spectra.

Table 1 shows an overview of the relevant spectral lines and their most important properties.

3. Pressure

The Optix was designed for pressures above $1{\cdot}10^{-6}$ mbar, and obtains an optimum optical resolution at pressures above $1{\cdot}10^{-4}$ mbar assuming mixtures of H_2, D_2, T_2, ^{3}He, ^{4}He, and Ne. The observed pressures for both installation position are shown in figure 2 top row for the OGA chamber and bottom row for the main roughing line. Each figure contains data from three pressure gauges as indicated in figure 1,

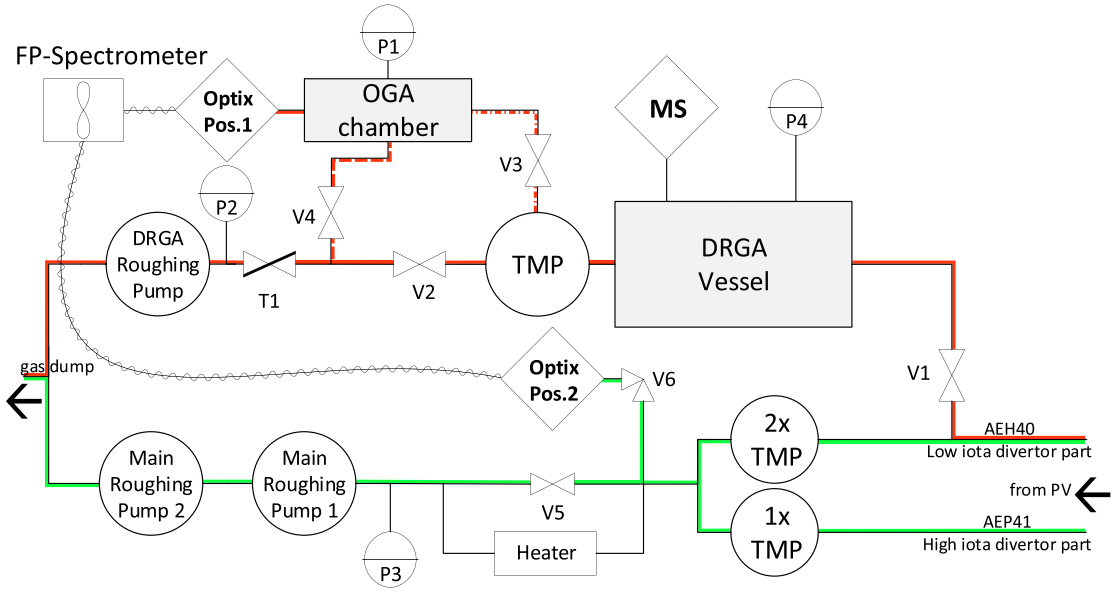

Figure 1. Schematic view of the relevant gas and fibre connections. Gas flows from the right (W7-X plasma vessel) to the left (gas dump). The initial position of the Gencoa OGA at the DRGA OGA vessel is indicated as Optix Pos.1, and the corresponding gas flow in denoted in red. The dash-dotted variant via V3 shows the connection to the TMP interstage port, the dashed variant via V4 shows the connection to the roughing line. The position at the main pumping system roughing line is indicated as Optix Pos.2, and the gas flow is given in green. The sine-waved line indicates an optical fibre. (colour online).

Table 1. List of relevant lines, their respective wavelength, relative intensity and transition probability. Data taken from the NIST ASD database [19]. Lines with asterisk denote Ritz wavelengths.

Species	λ (nm)	rel. intensity	A_{ki} (s^{-1})
Ar I	667.728	100	$2.3{\cdot}10^{5}$
O II	667.786	12	$3.37{\cdot}10^{6}$
He I	667.8151	100	$6.3705{\cdot}10^{7}$
Ne I	667.82 766	5000	$2.33{\cdot}10^{7}$
^{3}He I	667.865 433*	—	—
C I	667.9649*	—	$2.2{\cdot}10^{5}$

and the internal Optix pressure reading. Naturally, all total pressure measurements in vacuum have different (and sometimes quite significant) systematic uncertainties, so a direct comparison of pressures is potentially flawed. The pressure gauge at P2 is a compact Pirani gauge (Edwards APG100) near the roughing pump of the DRGA pumping system and might be suffering from saturation near its lower operation limit. The pressure gauge at P3 is a piezo/Pirani combined gauge (Pfeiffer RPT200) near the rouging pump of the main vacuum system, and has a nominal operation window from $1{\cdot}10^{-4}$ mbar to atmospheric pressure. All gauges are calibrated for nitrogen and were not re-calibrated for other gas mixtures.

While the total pressure achieved at the Optix was usually well above the pressures of the design phase, a significant fraction of the gas was residual atmospheric nitrogen (Optix Pos.1) or nitrogen for flushing the main vacuum TMPs (Optix Pos.2). The partial pressure of pumped plasma exhaust gases is thus much lower than the total pressure, and as the emission intensity for a given line to first order is proportional to the partial pressure, the line emission in those plasmas is much weaker than anticipated. This could at least partially be compensated by a longer integration time in the FPS camera, but significantly reduces the time resolution of the measurement. The combined partial pressures of all plasma gases are shown per program for an exemplary experiment day in the right hand side panels of figure 2. It was obtained by assuming a constant nitrogen background, and calculating the difference between the pressure value at the start of a plasma program and the maximum of the pressure up to 5 s after plasma program termination. The delay was introduced because the largest pressures in the exhaust are usually observed shortly after plasma termination, when plasma recombination and outgassing of hot plasma facing components produce a significant amount of gas, and the receded DRGA analysis chamber has a transfer time of >1 s [14].

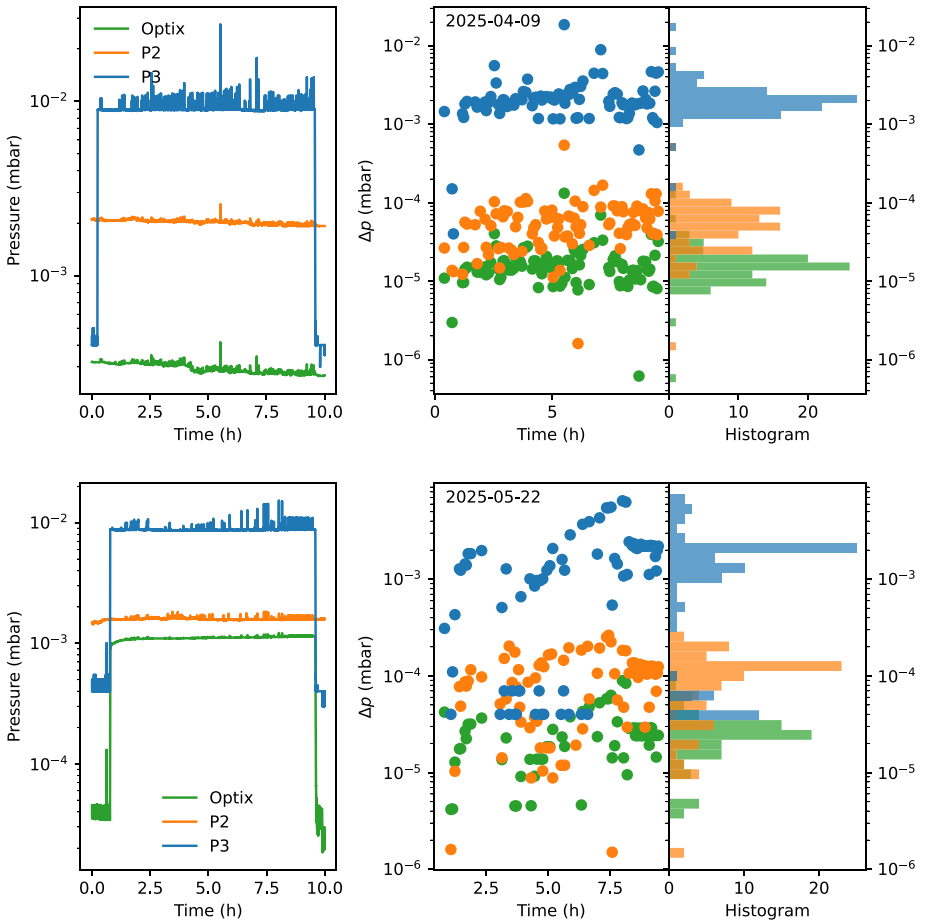

Figure 2. Comparison of pressures in the OGA feeding lines over one operation day for each of the mounting positions: Pos.1 in top row, Pos.2 in bottom row. Measurement position names as indicated in figure 1. left: Time trace of pressures over the operation day. Little spikes indicate plasma pumpout from the plasma vessel. The large pressure steps in P3 at the beginning and end of the experiment day are induced by the (de)activation of nitrogen flushing in the main vacuum TMPs. right: Pressure difference between the beginning of a W7-X plasma program and the maximum pressure achieved up to 5 s after program termination, and a histogram to the right hand side.

For the Optix at Pos.1 we see a significant mismatch between the measured total pressures of about a factor of 7, and between the measured exhaust gas pulses of about a factor of 5. For the Optix at Pos.2 we also see significant mismatches, here with a factor of 9 for the measured total pressures and a factor of 7 for the exhaust gas pulses.

While the total pressure measured inside the Optix increased significantly, the exhaust gas amount only increased very slightly. This was, however, enough to acquire a measurable signal, as shown in the next section.

4. He isotope measurement

Multiple experiments with ^{3}He injection were performed during OP2.3, with the main focus on the ion cyclotron resonance heating (ICRH) [16] minority heating. To detect the relative concentrations of helium isotopes, a number of ^{3}He and ^{4}He injection experiments were conducted specifically to test the He isotope distinction capabilities of the Optix. With the Optix still in Pos.1 no signal could be generated within the given restrictions of the experiment, regardless of integration time. After moving the Optix to Pos.2, we performed a dedicated experiment with alternating ^{3}He and ^{4}He gas puffs with increasing duration. As an example, we will discuss W7-X program 20 250 521.41 whose key quantities are shown in figure 3. It is a 15 s long plasma performed in the high-iota configuration and heated with 3 MV of electron cyclotron resonance heating (ECRH) [18]. A series of alternating ^{3}He and ^{4}He gas puffs was injected, where the latter were kept constant and the former were exponentially increasing to scan a range of concentrations. Due to the helium injections, the helium content of the plasma increased up to 60% and line integrated electron density rose to nearly $1{\cdot}10^{20}$ m^{-2}. Figure 4 shows the

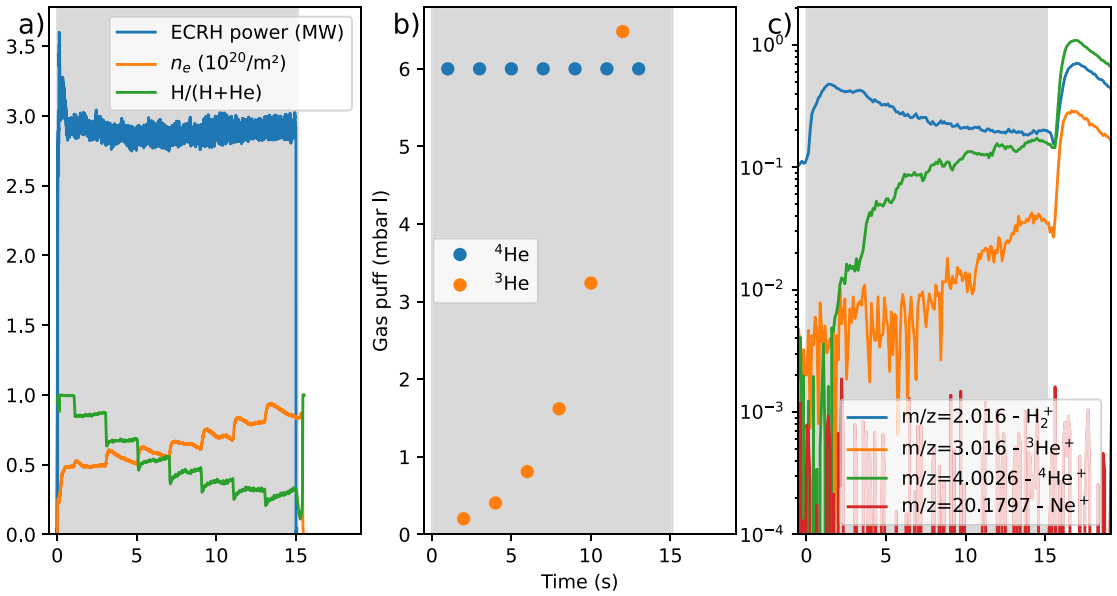

Figure 3. Overview of the W7-X program 20 250 521.41, with the plasma heating phase indicated in grey. Panel (a): ECRH heating power, line integrated density, and hydrogen to helium ratio from line-ratio spectroscopy [17]. Panel (b): Gas puff timing and magnitude for ^{3}He and ^{4}He. Panel (c): Measured raw intensities of different mass/charge ratios associated with the species of interest, as observed in the DRGA with a mass spectrometer. (colour online).

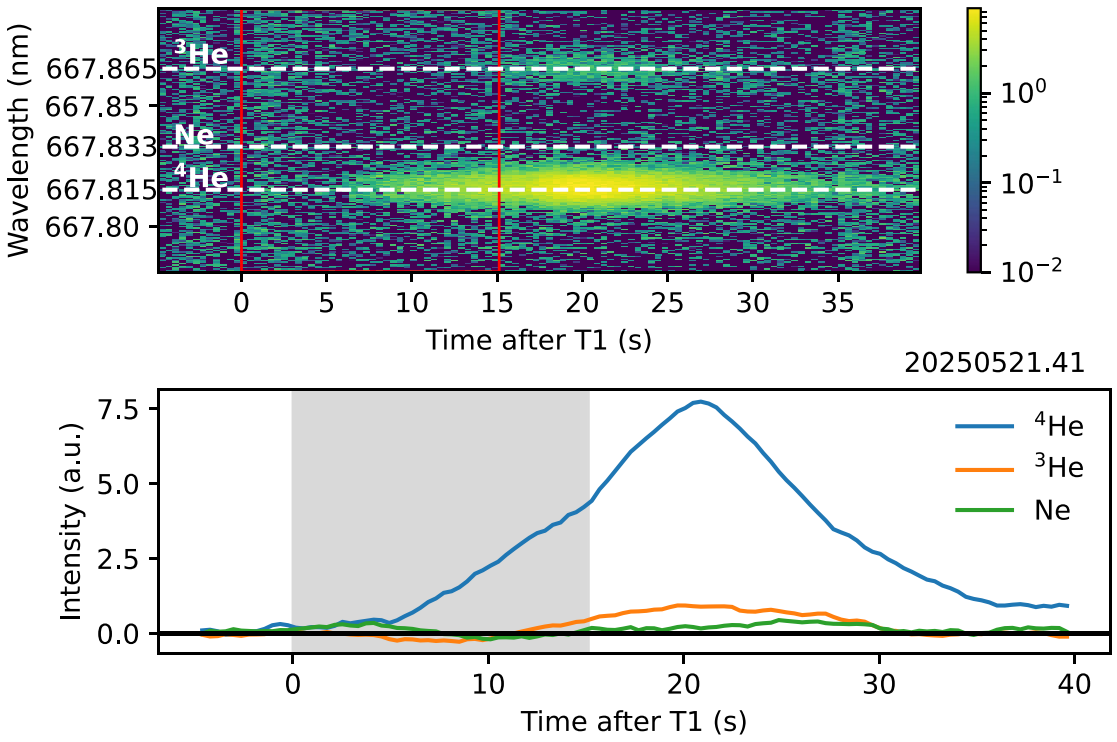

Figure 4. Measured spectra from W7-X program 20 250 521.41, which was fuelled with successively increasing gas puffs of ^{3}He and ^{4}He as shown in figure 3. top: Background-substracted intensity over wavelength and time, the plasma heating phase is indicated with a red rectangle. Expected line centres are shown with a white dashed line. Bottom: Time evolution of the three line centres of interest. The plasma heating phase is indicated as a grey-shadowed region.(colour online).

Optix measurement, with the full spectrum in the top panel and the evolution of the lines in question in the bottom panel.

The helium content of the plasma shows very pronounced steps while increasing, and the DRGA data shows a resemblance of these steps as well, but much less pronounced already. The Optix measurement of ^{4}He shows the same overall trend, but no time resolution of the injection is visible.

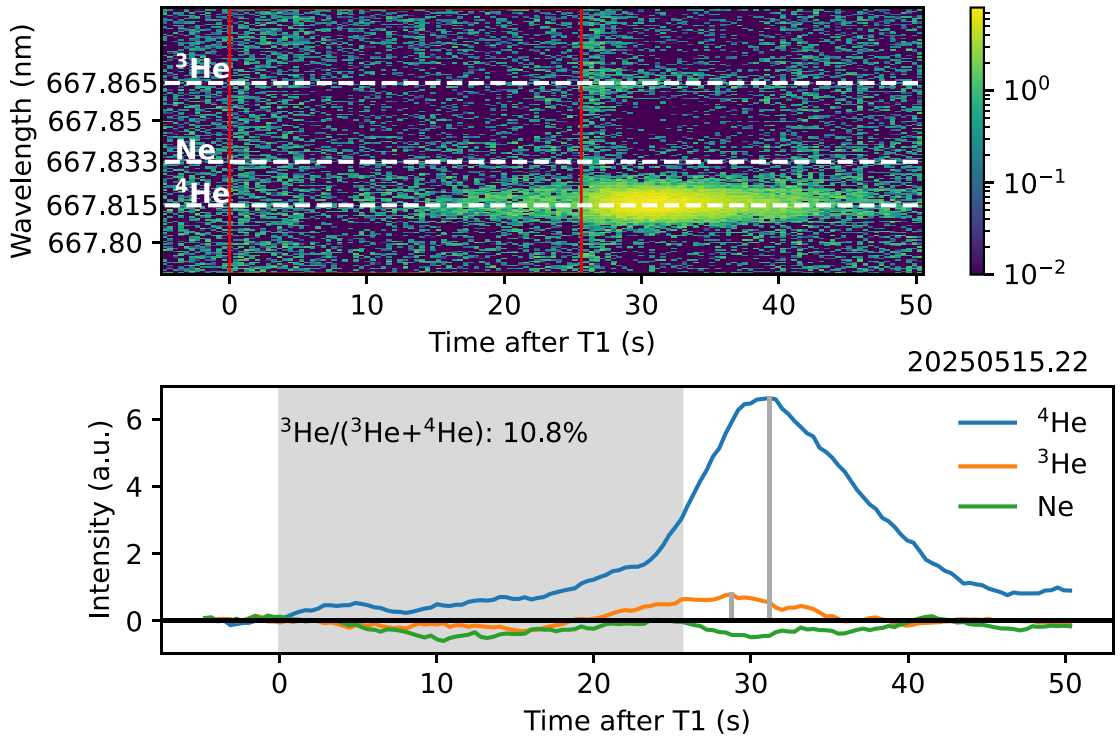

Figure 5. Measured spectra from W7-X program 20 250 515.22, an ICRH minority heating program. Albeit faint, the ^{3}He signal is visible and the estimated ratio of 10% matches the design point of the gas program. Panels as described in figure 4.(colour online).

Furthermore, the signal continues to increase with only a slight change in slope after plasma termination, where we expect the neutralized plasma being pumped out. The ^{3}He signal follows the trend of ^{4}He in both isotope-resolving measurements, but at a lower magnitude and without visible steps. There is no measurable amount of neon detected in the DRGA, thus the Ne line in figure 4 can be considered noise.

This shows that we can spectroscopically distinguish helium isotopes, but the current setup is not capable of delivering a time resolution at par with the existing mass spectrometry diagnostic. The issue is not so much a shortcoming of the Optix system itself, but the connection to the gas flow of the plasma which needs to be both well compressed and timely, to achieve signals with usable fidelity.

An application to the ICRH three-ion heating scheme is shown in figure 5, where about 10%^{3}He in ^{4}He was measured. This matches well with the target composition, as well as measured data from mass spectrometry.

5. Plasma spectroscopy

The FPS was designed for the observation of a closely controlled low-temperature plasma with only weak magnetic field. Due to the availability of sightlines into the W7-X plasma, we conducted a test of the spectrometer on a core sightline and on an edge sightlines. The experiments conducted and results thereof are reported in this section.

5.1. Sightline through the plasma core

During ^{3}He injection tests a line broadening of the helium line at 667.8 nm was observed in an overview spectrometer observing the plasma from the outer midplane through the plasma core. This prompted the question whether the FPS would be capable of resolving the assumed isotopic line split. The FPS was set up to operate on the given fibre with a 400 μm core and a NA = 0.22, and observed the plasma for four experimental sessions via the W7X port AEM41. A strong, but varying background was observed, with pronounced features to either side of the spectral range. This was strongly correlated with the plasma heating phase and is thus at least partially attributed to plasma background.

In an attempt to identify the featured adjacent to the specified spectral range a spectrum was stitched from the manual analysis software by moving the ROI horizontally. The example raw data and original

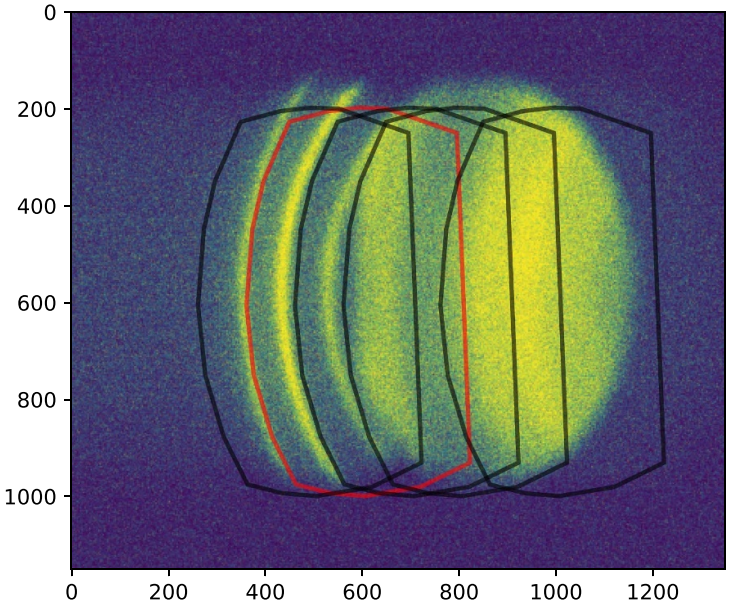

Figure 6. Raw image of 20 250 508.11 (contrast enhanced) overlayed with the ROIs used to create the spectra shown in figure 7. The original ROI is indicated in red, other ROIs shifted by (−100, 100, 200, 300, 400)px are given in black.(colour online).

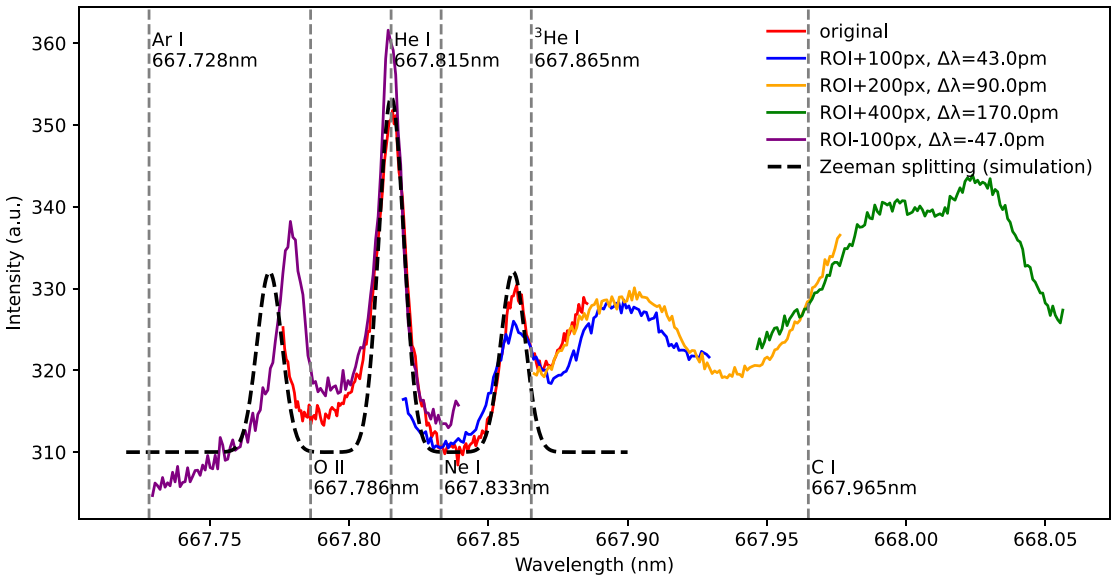

Figure 7. Spectra obtained from the core plasma sightline with different shifted ROIs. The shift is indicated in pixel, and the manually adjusted wavelength is given along with the shift. Candidate lines from [19] are given in grey dashed lines, annotated with the origin species and tabulated wavelength. The black dashed line shows a simulated Zeeman splitting of the He I line with an magnetic field strength of 2.1 T and an incidence angle of 85 $^{\mathrm{circ}}$.

and shifted ROIs are shown in figure 6, and the resulting stitched spectrum along with adjacent candidate lines in figure 7. The wavelength of the spectrum is adjusted to match the ^{4}He I line at 667.815 nm and shifted spectra are adjusted to make an approximate match in the overlap areas. The indicated candidate lines do not align well with the observed shapes, which might only be partially attributed to Doppler shift. A more likely explanation is line splitting of the ^{4}He I line by Zeeman splitting, as described in [20, 21]. A simulation of split line with an angle of 85° and a magnetic field strength of 2.1 T shows a reasonable agreement with the observed line-like features. Additionally, an influence of higher orders from the Fabry–Perot interferogram is expected to contribute to the overall spectrum. Therefore, an attribution of the observed signals is only partially possible.

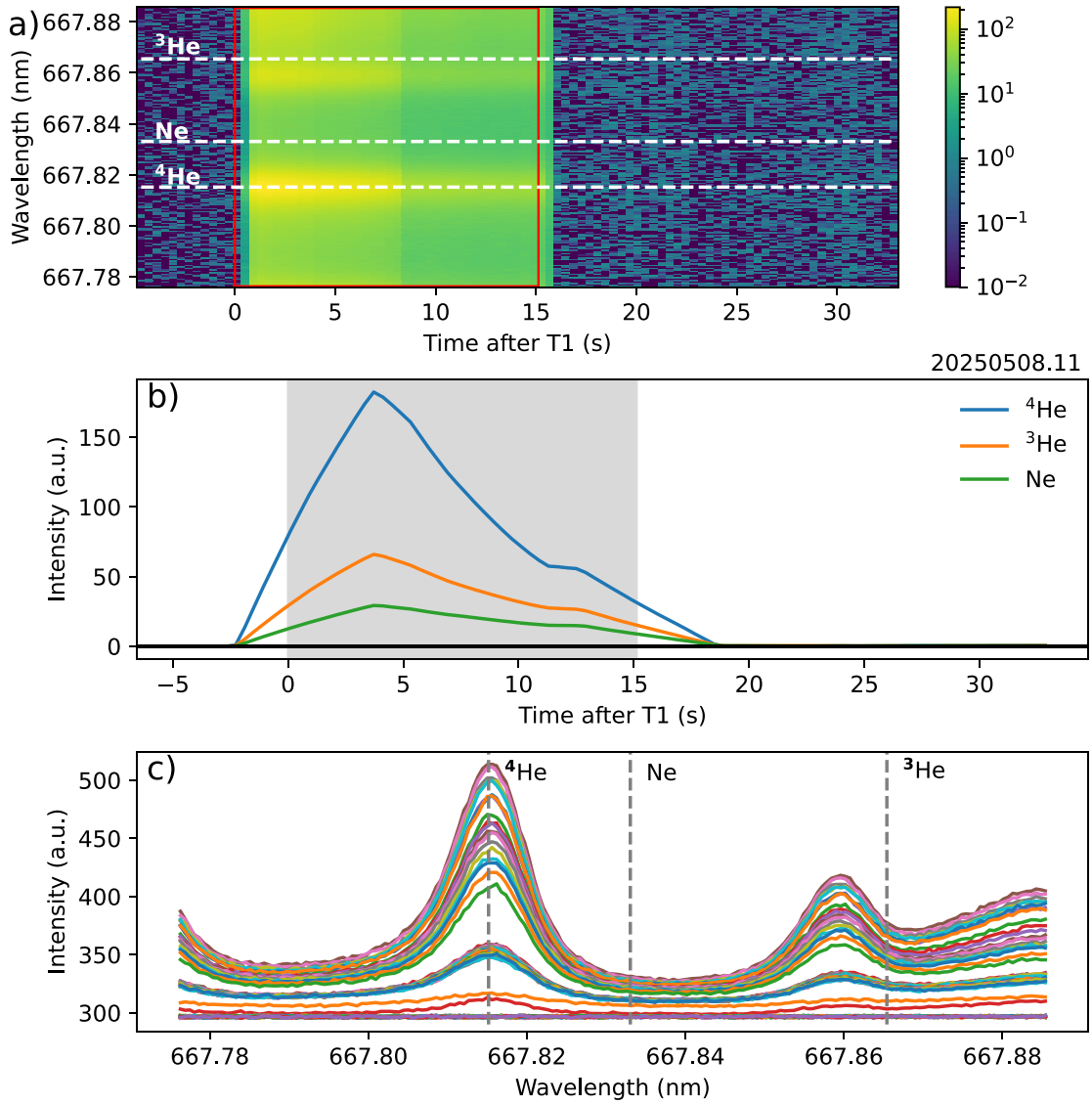

Figure 8. Exemplary measurement from the core plasma sightline with a visible He I line, a line close to the expected ^{3}He I line and the plasma background features at high and low wavelength boundary of the spectral range. Panel (a): Measurement overview as in figure 4. Panel (b): Intensity over time for three relevant wavelengths. The signals do not necessarily represent the presence of indicated species. Panel (c): Plot of all spectra altogether. Besides the dominating He I line the extra line near the expected ^{3}He I and the plasma background features and sigma components from the Zeeman splitting at high and low wavelengths can clearly be seen.

With a more He-rich plasma the observed spectra were dominated by the He I line, but the background to either side did not disappear. The He I line intensity shows clear modulation with the measured plasma He concentration, and the plasma background varies with plasma density. An example measurement is shown in figure 8, where all of the mentioned features are clearly visible.

The remarkable line-like feature at 667.86 nm near the expected ^{3}He I line appeared despite no ^{3}He was injected. This was consistently observed, and indicates that despite the proximity to an existing line the feature is not connected to ^{3}He. The absence of ^{3}He was also confirmed via mass spectrometry.

5.2. Sightline through the plasma edge

An edge spectroscopy sightline observing the newly installed upstream He-beam used during experiments with an He–Ne mixture injection with the goal of spectrally resolving He I at 667.81 nm and Ne I at 667.83 nm. The He–Ne mixture was prepared with a mixing ratio of 4:3, but no direct measurement of the injected gas composition was performed.

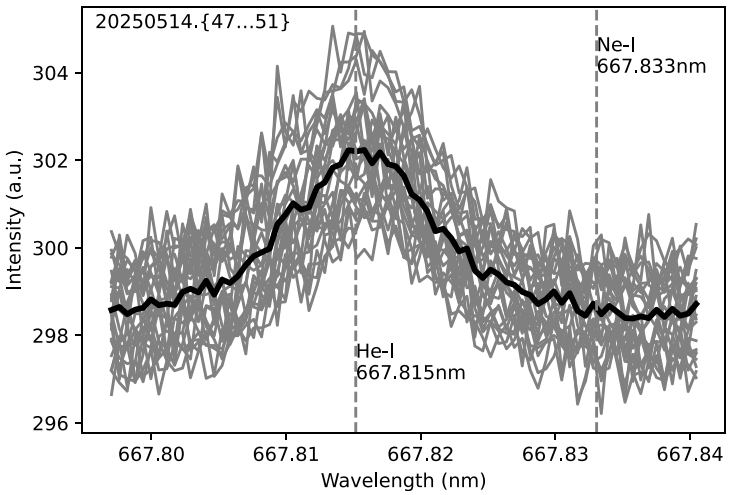

Figure 9. All spectra (grey) with significant He I line from the programs 20 250 514.47. . . 51 with He–Ne gas mix injection at the midplane gas inlet. The averaged spectrum is shown in black, and expected line centres are indicated with dashed lines. While the He I signal is visible above noise, the Ne I line can not be distinguished from the noise.

The gas mixture was injected into four plasma programs with seven pulses of 150 ms length at a gas reservoir pressure of 47 mbar, yielding hardly any perturbation of the plasma due to the small amount of gas injected. In a following program, the gas was injected continuously for 2 s, which emptied the gas reservoir nearly completely.

From the resulting data all spectra with a visible He I line were selected and averaged. The result is shown in figure 9. A small He I signal can be seen, but there is no signal for Ne I to be observed from the acquired data.

6. Conclusion

We have shown the first field test of the Optix, and could successfully demonstrate the spectroscopically assisted isotope composition measurement of the exhaust stream in an operating fusion experiment. The results of this test with ^{3}He and ^{4}He are promising, and should be extended to H, D and T, as their accounting is crucial for a fusion reactor. Great care is to be taken for the design of the gas supply of the Optix. To achieve the desired goals of a sufficient time resolution in the order of 1 s and sensitivity below 1% the gas stream needs to be sufficiently compressed and ideally be free of additional gases. Contrary to mass spectrometers, an OGA requires a large gas throughput to achieve full diagnostic capabilities. This challenges the envisaged concept of an exhaust gas analysis by chained analysers—mass spectrometer and OGA—on the same gas stream, and a split of these two technologies might be warranted for the benefit of both of them.

The time resolution of the isotope measurement could not be determined within this field test, as the gas sampling conditions did not allow sufficiently clear signals. With an improved sampling position, ideally without nitrogen admixture, this is expected to improve significantly. With these improvements, an OGA with such a high-resolution spectrometer promises to give access to ideally real-time isotopic composition measurement in the exhaust stream with a device much less sensitive to fringing magnetic field than comparable methods, such as mass spectrometers.

The application of the FPS to the observation of the high-temperature plasma of W7-X was only partly successful. While some He I could be measured, and parts of the features are at least qualitatively explained with Zeeman splitting, some features of the spectra remain unclear and the benefits of relatively constant low-temperature plasma discharge for gas composition measurement as found in the remote plasma generator become very obvious.

Acknowledgments

This project has been supported by UK Atomic Energy Authority (UKAEA) though the Fusion Industry Programme (FIP). The FIP is stimulating the growth of the UK fusion ecosystem and preparing it for

the future global fusion power plant market. More information about the FIP can be found online; https://ccfe.ukaea.uk/programmes/fusion-industry-programme/.

This work has been carried out within the framework of the EUROfusion Consortium, funded by the European Union via the Euratom Research and Training Programme (Grant Agreement No 101052200 — EUROfusion). Views and opinions expressed are however those of the author(s) only and do not necessarily reflect those of the European Union or the European Commission. Neither the European Union nor the European Commission can be held responsible for them.

Data availability statement

The data cannot be made publicly available upon publication because they contain commercially sensitive information. The data that support the findings of this study are available upon reasonable request from the authors.

ORCID iDs

G Schlisio 0000-0002-5430-0645
M Law 0000-0002-2165-5503
C C Klepper 0000-0001-9107-8337
E Delabie 0000-0001-9834-874X
P Zs Pölöskei 0000-0001-7781-5599
Y M Boumendjel 0009-0009-3480-3964
F B T Siddiki 0000-0002-0474-300X
M Krychowiak 0009-0001-4141-5558

References

[1] Brindley J *et al* 2024 *Proc. IFHTSE*
[2] Brindley J *et al* 2025 *Proc. SOFE*
[3] Wade M R *et al* 1995 *J. Nucl. Mater.* **220** 178–82
[4] Hillis D L, Morgan P D, Ehrenberg J K, Groth M, Stamp M F, von Hellermann M and Kumar V 1999 *Rev. Sci. Instrum.* **70** 359–62
[5] Klepper C C, Biewer T M, Marcus C, Andrew P, Gardner W L, Graves V B and Hughes S 2017 *J. Instrum.* **12** C10012
[6] Colchin R J, Hillis D L, Maingi R, Klepper C C and Brooks N H 2003 *Rev. Sci. Instrum.* **74** 2068–70
[7] Grulke O *et al* 2024 *Nucl. Fusion* **64** 112002
[8] Grulke O *et al* IAEA FEC 2025
[9] Ongena J *et al* 2020 *AIP Conf. Proc.* **2254** 070003
[10] Kazakov Y *et al* 2017 *Nat. Phys.* **13** 973–8
[11] Vartanian S *et al* 2021 *Fusion Eng. Des.* **170** 112511
[12] Hernandez G 1986 *Fabry-Perot Interferometers* (Cambridge University Press)
[13] Grahl M *et al* 2017 *Fusion Eng. Des.* **123** 1015–9
[14] Schlisio G, Klepper C C, Harris J H, Biewer T M, Winters V R, Wenzel U, Kornejew P, Laqua H and Krychowiak M 2019 *Rev. Sci. Instrum.* **90** 093501
[15] Schlisio G, Ravelli F A, Klepper C C, Harris J H, Biewer T M, Marcus C, Kharwandikar A K, Naujoks D and Kremeyer T 2022 *IEEE Trans. Plasma Sci.* **50** 4120–5
[16] Ongena J *et al* 2023 *Fusion Eng. Des.* **192** 113627
[17] Ford O *et al* 2024 *Rev. Sci. Instrum.* **95** 083526
[18] Laqua H P *et al* 2023 *EPJ Web Conf.* **277** p 04003
[19] 2024 NIST Atomic Spectra Database (https://doi.org/10.18434/T4W30F)
[20] Gradic D *et al* 2021 *Nucl. Fusion* **61** 106041
[21] Gradic D, Krychowiak M, König R, Henke F, Otte M, Perseo V and Pedersen T S (W7-X Team) 2022 *Plasma Phys. Control. Fusion* **64** 075010